Supplementary Information

Structure determination and magnetic properties of the Mn-doped MAX phase Cr_2GaC

Jan P. Siebert[a], Shayna Mallett[a], Mikkel Juelsholt[b], Hanna Pazniak[c], Ulf Wiedwald[c], Katharine Page[d,e], Christina S. Birkel[*a,f]

X-ray diffraction

XRD data was obtained using a 2nd generation D2 Phaser (Bruker) with Cu $K_{\alpha1,2}$ radiation and a 1D SDD LYNXEYE detector (Bruker). The refinement was carried out in Topas[1]. Generally, a sample displacement factor, scale factor, background, lattice parameters, and phase compositions were refined. In order to determine accurate lattice parameters, LaB_6 (NIST standard) was mixed into the sample, so that both LaB_6 and $(Cr_{1-x}Mn_x)_2GaC$ main peaks had similar intensities. These scans were used to refine the lattice parameters of $(Cr_{1-x}Mn_x)_2GaC$. In a separate refinement of data without LaB_6 contributions, the previously determined $(Cr_{1-x}Mn_x)_2GaC$ lattice parameters were used and not further refined. This second refinement gave the phase composition values shown in the study.

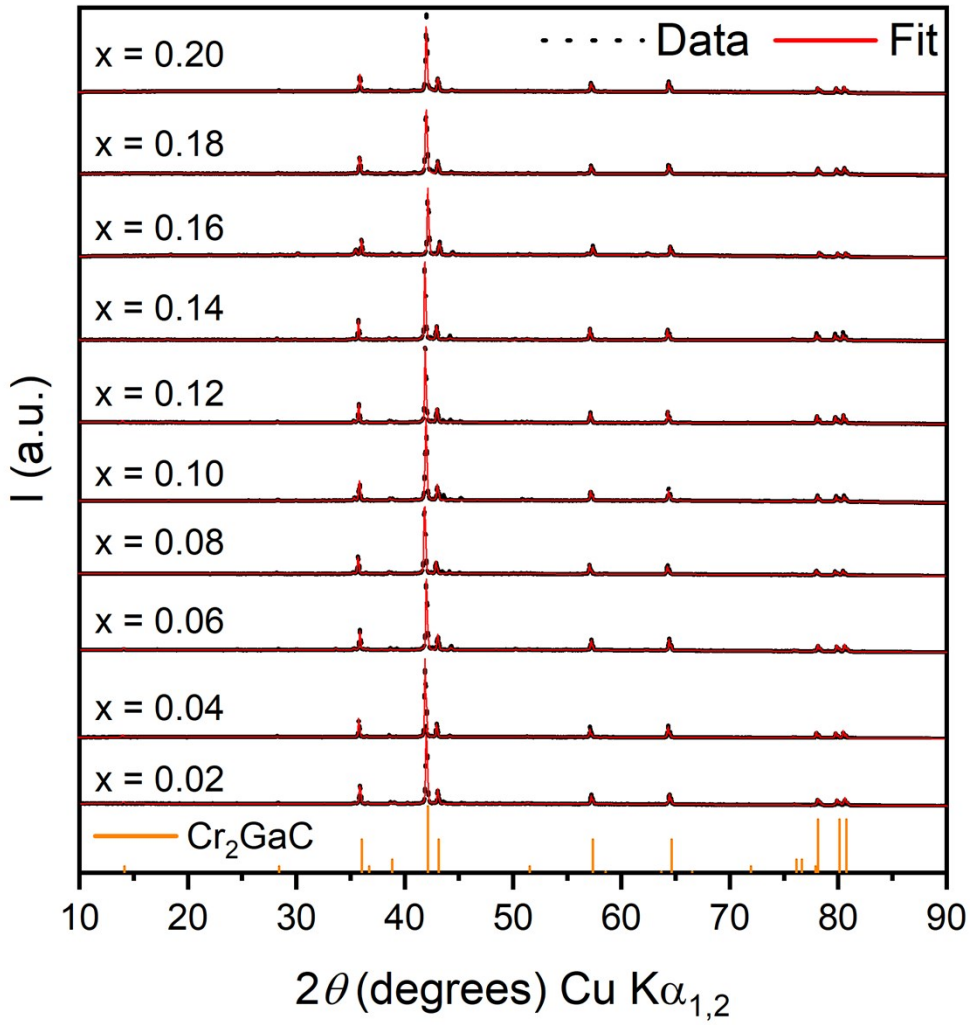

Figure S1: X-ray powder diffraction data (black dots) and Rietveld refinements (red lines) of all $(Cr_{1-x}Mn_x)_2GaC$ samples prepared in this study (x = 0.02 – 0.2). Reflection markers for Cr_2GaC intensities are shown in orange.

Table S1: Results from the Rietveld refinement of the XRD data of $(Cr_{1-x}Mn_x)_2GaC$ (x =0.02 -0.2) that include LaB_6 as an internal standard: Lattice parameters, and figures of merit (R_{wp}, GOF). Calculated errors are provided in parentheses.

Mn content /at-%	*a* /Å	*c* /Å	V /Å³	R_{wp}	GOF
0 (literature)[2]	2.88(6)	12.61(6)	92.05	-	-
2	2.89224(6)	12.6105(5)	91.355(5)	7.06	1.29
4	2.89251(7)	12.6125(5)	91.387(6)	9.30	1.59
6	2.89245(7)	12.6110(5)	91.372(6)	6.30	1.16
8	2.89320(6)	12.6098(5)	91.410(5)	6.87	1.38
10	2.89363(7)	12.6091(5)	91.433(6)	5.99	1.01
12	2.8937(2)	12.6059(8)	91.414(9)	9.57	1.66
14	2.89354(4)	12.6088(4)	91.424(4)	5.78	1.00
16	2.89366(5)	12.6104(4)	91.443(4)	5.92	1.12
18	2.89384(9)	12.6100(7)	91.452(8)	9.62	1.64
20	2.89394(8)	12.6066(6)	91.434(6)	9.70	1.73

Table S2: Results from the Rietveld refinement of the XRD data of $(Cr_{1-x}Mn_x)_2GaC$ (x =0.02 -0.2) without

Mn content/ at-%	Confirmed compounds (wt-%)
2	Cr_2GaC (80.2); Cr_3C_2 (19.8)
4	Cr_2GaC (83.2); Cr_3C_2 (8.1); $Mn_{23}C_6$ (8.7)
6	Cr_2GaC (71.7); Cr_2O_3 (8.9); $MnCr_2O_4$ (7.1); $Mn_{23}C_6$ (12.4)
8	Cr_2GaC (76.7); Cr_3C_2 (10.1); $MnCr_2O_4$ (8.0); $Mn_{23}C_6$ (5.2)
10	Cr_2GaC (77.2); $Mn_{23}C_6$ (4.9); Cr_3C_2 (9.4); $MnCr_2O_4$ (8.4)
12	Cr_2GaC (90.2); $MnCr_2O_4$ (9.8)
14	Cr_2GaC (73.3); Cr_3C_2 (7.4); $MnCr_2O_4$ (5.8); $Mn_{23}C_6$ (13.4)
16	Cr_2GaC (51.7); $MnCr_2O_4$ (26.3); $Mn_{23}C_6$ (8.8); Cr_2O_3 (5.6); Cr_3C_2 (7.7)
18	Cr_2GaC (66.0); $Mn_{23}C_6$ (2.4); Cr_3C_2 (10.3); Cr_7C_3 (22.0)
20	Cr_2GaC (67.5); $Mn_{23}C_6$ (3.8), CrC (2.1), CrO_2 (20.9), MnO (5.7)

LaB_6: confirmed phases and weight fractions for each sample.

STEM imaging

STEM images for selected samples of the doping series (captions refer to nominal doping amount). The spherical/elliptical shape of the particles as well as the size distribution of the MAX phase particles is clearly visible.

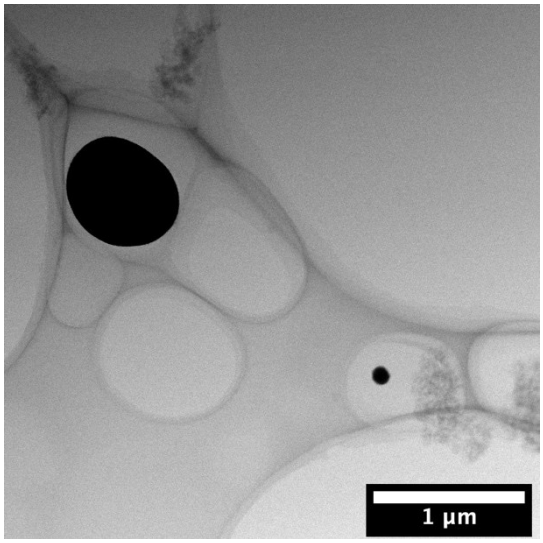

Figure S2: STEM BF micrograph of 4 at-% Mn doped Cr_2GaC particles.

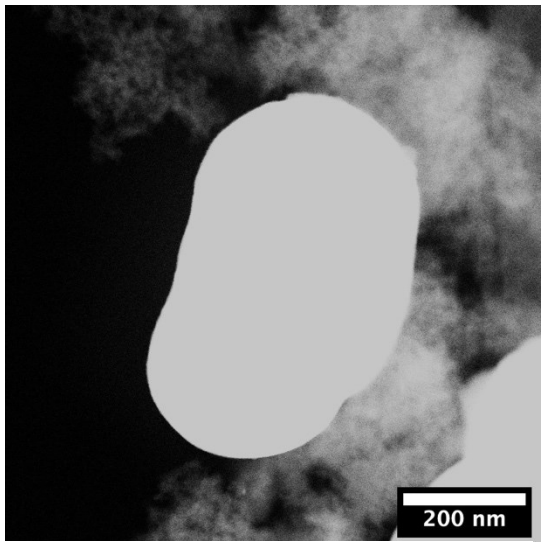

Figure S3: STEM HAADF micrograph of 8 a-t% Mn doped Cr_2GaC particles.

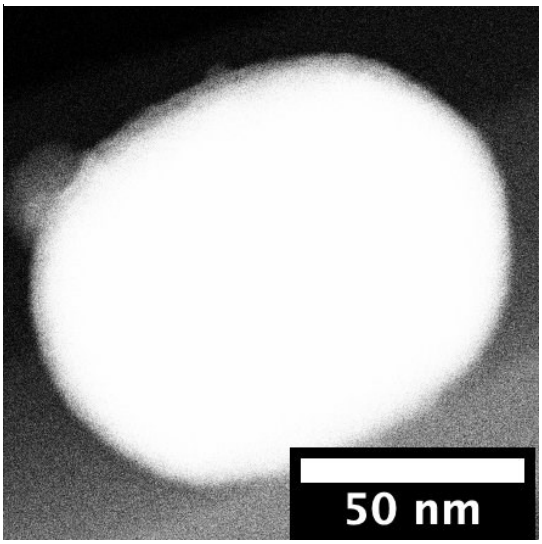

Figure S4: STEM HAADF micrograph of a 12 at-% Mn doped Cr_2GaC particle.

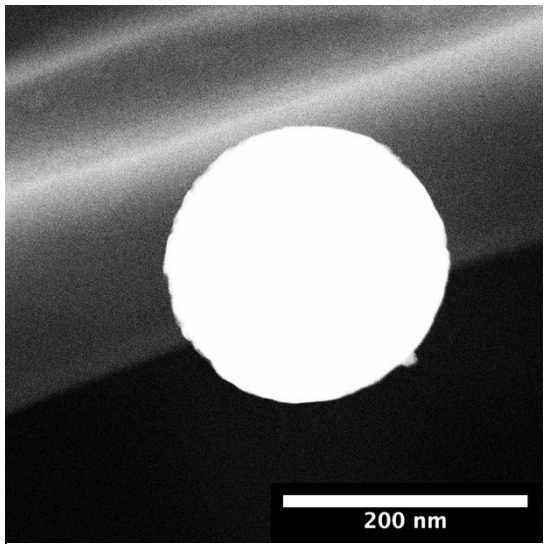

Figure S5: STEM HAADF micrograph of a 16 at-% Mn doped Cr_2GaC particle.

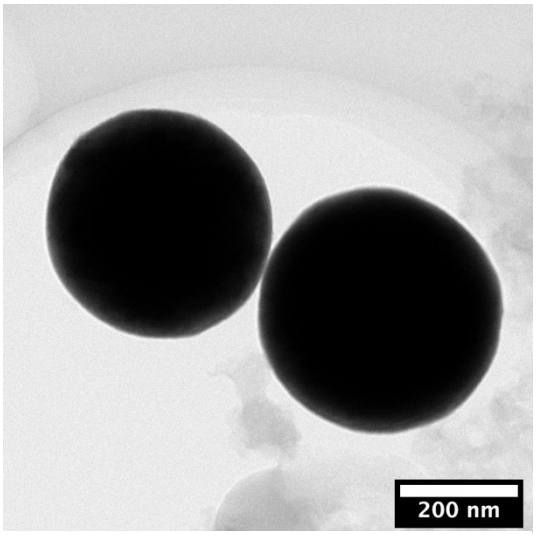

Figure S6: STEM BF micrograph of 18 at-% Mn doped Cr_2GaC particles.

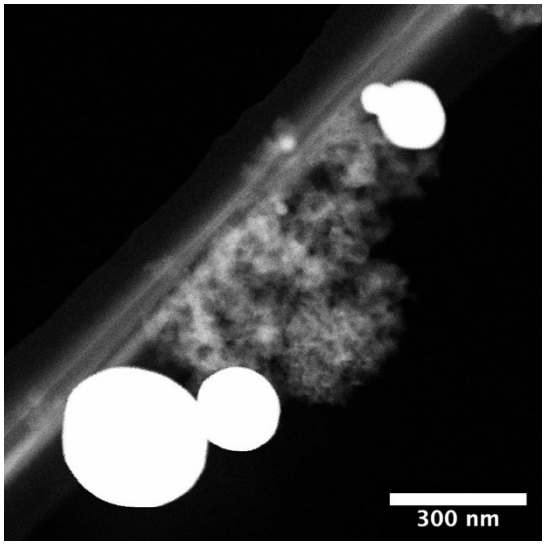

Figure S7: STEM HAADF micrograph of 20 at-% Mn doped Cr_2GaC particles.

The following shows the detected, and averaged, atomic percentages for the elements Cr, Ga, and Mn resulting from EDS analysis. For each sample multiple particles were investigated. The right-most column displays the Mn-percentage detected out of the amount used (e.g. at a nominal amount of 4 at-% Mn, only 2.4 at-% could be detected in MAX phase particles, which equals 60% of expected nominal value). Based on the number of particles, the standard deviation for each elemental quantification was calculated (Table S3). For the most part, the error is around 1, which is similar to the reasonably assumable measurement error of 1%. Particularly Mn is very consistent, suggesting a very homogenous distribution of Mn in each sample. The larger deviations particularly in the x = 0.04 sample in the Cr and Ga quantifications can be explained with small amounts of Cr_3C_2 being attached to the MAX phase particle.

Table S3: Results from the STEM analysis: Calculated at-% averages for $(Cr_{1-x}Mn_x)_2GaC$ (x =0.04 - 0.2). Standard deviation for each element and doping increment given in parentheses.

At-% Mn	Avg. Cr at-%	Avg. Ga at-%	Avg. Mn at-%	% Mn detected	# of particles
4	65.53 (4.9)	32.03 (5.2)	2.40 (0.49)	80	4
8	65.11 (0.83)	29.33 (0.5)	5.57 (0.85)	70	6
12	60.11 (0.49)	31.31 (0.42)	8.58 (0.46)	72	6
14	60.90 (1.14)	28.27 (1.4)	10.83 (1.02)	77	6
16	59.58 (1.0)	29.50 (0.53)	10.93 (1.36)	68	7
18	55.71 (0.84)	31.80 (1.04)	12.49 (0.85)	69	13
20	57.23 (1.53)	32.26 (1.97)	10.51 (0.99)	53	4

Neutron diffraction data

Neutron time-of-flight data was obtained at the Nanoscale-Ordered MAterials Diffractometer, NOMAD, and measured on 4 detector banks at room temperature. Rietveld refinement was carried out in Topas academic on all 4 banks simultaneously. A scale factor and zero error for each crystalline structure were refined individually for each bank. All other structural parameters were constrained to be the same on all banks. The structural parameters are seen in Table S1, S2, S3 and S4. In general, the unit cell, atomic positions and the atomic displacement parameters were refined. On Mn and Cr site the Mn/Cr occupancy ratio was refined with the total occupancy assumed to be 1. The peak shapes

used was the time-of-flight pseudo-Voigt determined for NOMAD. All other instrument parameters have been fixed to values determined from a LaB_6 standard refinement[3].
For the x = 0.04 sample the background was described using a 12th degree Chebyshev polynomial for each bank. For the x = 0.2 sample the background was described using a 20th degree Chebyshev polynomial for each bank. As discussed in the main text and shown in the section about PDF the samples contain a nanostructured carbon phase which gave rise to the low period oscillating background and the high order polynomial was needed to obtain a reasonable fit. The unknown phase at 2.2 $Å^{-1}$ present in Bank 1 and 2 was described using pseudo-Voigt peak in each bank, because the peak interfered with the background polynomial.

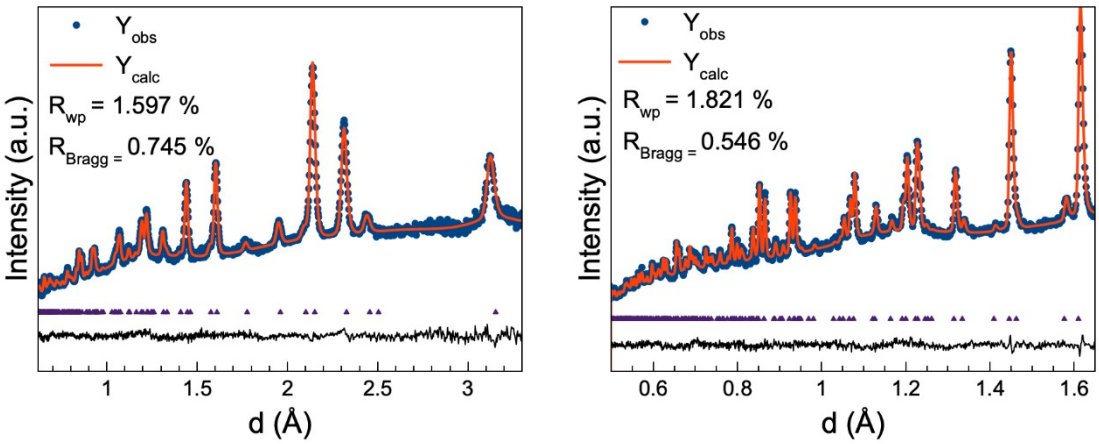

Figure S8: The remaining two neutron diffraction banks for the x = 0.04 sample, the 65 degree bank (left) and the 120 degree bank (right), and the resulting Rietveld refinements. Data shown in blue, fit in red and the difference between the two in black. The ticks indicate the Bragg peak positions.

Table S4: Refined parameters for the $(Cr_{1-x}Mn_x)_2GaC$ phase with x = 0.04.

	$(Cr/Mn)_2GaC$	**Space group**	**$P6_3/mmc$**		
	x	**y**	**z**	**Biso ($Å^2$)**	**Occ**
Ga	2/3	1/3	0.25	0.57	1
Cr	1/3	2/3	0.0856	0.328	0.967
Mn	1/3	2/3	0.0856	0.328	0.033
C	0	0	0	0.533	1
a	2.8982 Å				
b	2.8982 Å				
c	12.613 Å				
Global R_{wp}	1.700 %				
Bank	**1**	**2**	**3**	**4**	
R_{Bragg}	0.933 %	0.745 %	0.546 %	0.0195 %	
R_{wp}	1.833 %	1.597 %	1.821 %	1.648 %	

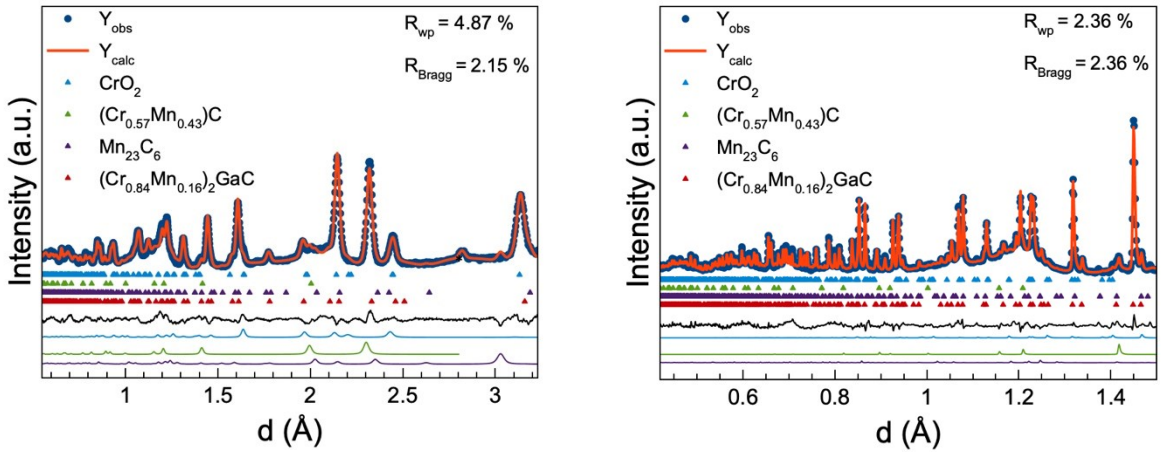

Figure S9: The remaining two neutron diffraction banks for the x = 0.2 sample, the 65 degree bank (left) and the 120 degree bank (right), and the resulting Rietveld refinements. Data shown in blue, fit in red and the difference between the two in black. The ticks indicate the Bragg peaks positions of the three phases. MnO_2 at the top, $(Cr_{0.57}Mn_{0.43})C$ in the middle and $(Cr_{0.84}Mn_{0.16})_2GaC$ at the bottom. The two curves in the bottom show the contribution from MnO_2 (purple) and $(Cr_{0.57}Mn_{0.43})C$ (green) after removal of the background.

Table S5: Refined parameters for the $(Cr_{1-x}Mn_x)_2GaC$ phase with x = 0.2.

	$(Cr/Mn)_2GaC$	**Space group**	**P63/mmc**		
	x	**y**	**z**	**Biso (Å²)**	**Occ**
Ga	2/3	1/3	0.25	0.927	1
Cr	1/3	2/3	0.0843	0.851	0.84
Mn	1/3	2/3	0.0843	0.851	0.16
C	0	0	0	0.766	1
a	2.8981 Å				
b	2.8981 Å				
c	12.6422 Å				
R_{wp}	5.1 %				
Bank	**1**	**2**	**3**	**4**	
R_{Bragg}	0.88 %	2.28 %	3.00 %	2.55 %	
R_{wp}	4.291	5.537	5.741	4.959 %	

Table S6: Refined parameters for the MnO_2 phase in the x = 0.2 sample.

	MnO_2	**Space group**	**Pnnm**		
	x	**y**	**z**	**Biso (Å²)**	**Occ**
Mn	0	0	0	0.739	1
O	0.400	0.400	0	3.00	1
a	4.455 Å				
b	4.434 Å				
c	2.913 Å				
R_{wp}	5.1 %				
Bank	**1**	**2**	**3**	**4**	
R_{Bragg}	1.66 %	3.30 %	4.79 %	4.24 %	
R_{wp}	4.291	5.537	5.741	4.959 %	

Table S7: Refined parameters for the (Cr/Mn)C phase in the x = 0.2 sample.

	(Cr/Mn)C	Space group	Fm-3m		
	x	**y**	**z**	**Biso (Å²)**	**Occ**
Cr	0.5	0.5	0.5	0.200	0.57
Mn	0.5	0.5	0.5	0.200	0.43
O	0.400	0.400	0	0.709	1
a	4.006 Å				
b	4.006 Å				
c	4.006 Å				
Global R_{wp}	5.1 %				
Bank	**1**	**2**	**3**	**4**	
R_{Bragg}	1.66 %	3.30 %	4.79 %	4.24 %	
R_{wp}	4.291	5.537	5.741	4.959 %	

Total Scattering and Pair Distribution Function

Pair Distribution Functions (PDFs) were obtained from the neutron time-of-flight data obtained at NOMAD using the in-house program ADDIE[4] for background subtraction and normalizations. The Fourier transform into the PDFs was done using pdfgetN3[5,6].

On the left in Figure S10 is the neutron PDF of the nominal 20 at-% Mn sample. As it can be seen on the right in Figure S10 that the long-range structure above 10 Å can be described using the same models as in the Rietveld refinement. However, extending the fit below 10 Å (Figure S11) the crystalline models fail to describe the local structure. The first peak appearing in the PDF is at 1.42 Å, which is too short for metal oxides or metal carbides. Instead, it fits well with the C-C distance in graphite. Figure S12 shows a fit with the three crystalline phases and a spherical graphite phase with a 7 Å particle diameter. Including this nanostructured phase results in a good fit of the local structure. The fit can be further improved by letting the carbon atoms move along the crystallographic *c*-axis, see Figure S13. The *c*-axis of the hexagonal graphite unit cell is elongated, which could explain the peak at 1.8 $Å^{-1}$ as described in the main text. From these fits it is clear that there is a nanostructured graphite-like carbon phase present which must originate from the carbon species, citric acid, used in the reaction.

There are no changes in the structural parameters in the crystalline phases between the long range and local structure fits, which means that there is no detected local structure disorder in the MAX phase.

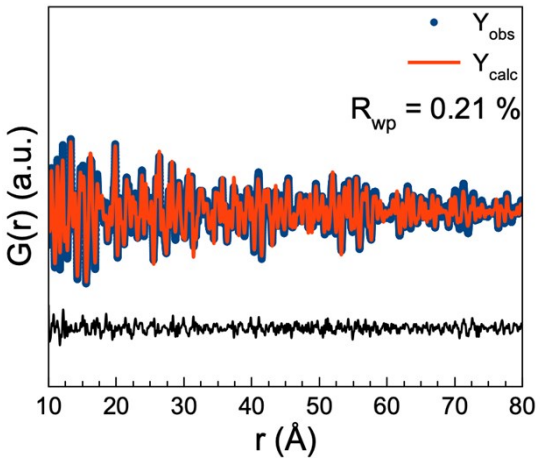

Figure S10: Neutron PDF of $(Cr_{1-x}Mn_x)_2GaC$ phase with x = 0.2. The PDF can be fitted using the same 3 crystalline phases used in the Rietveld refinement as seen in Table S13-S15.

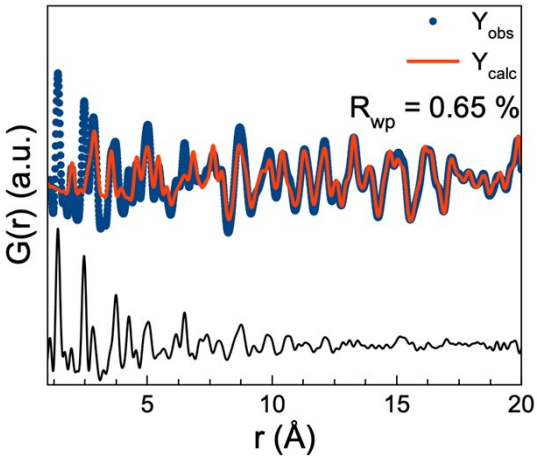

Figure S11: The same fit as shown in Figure S10, but extended below 10 Å. The fit fails below 10 Å, which means that beside the 3 crystalline phases, there is an additional nanostructured phase present.

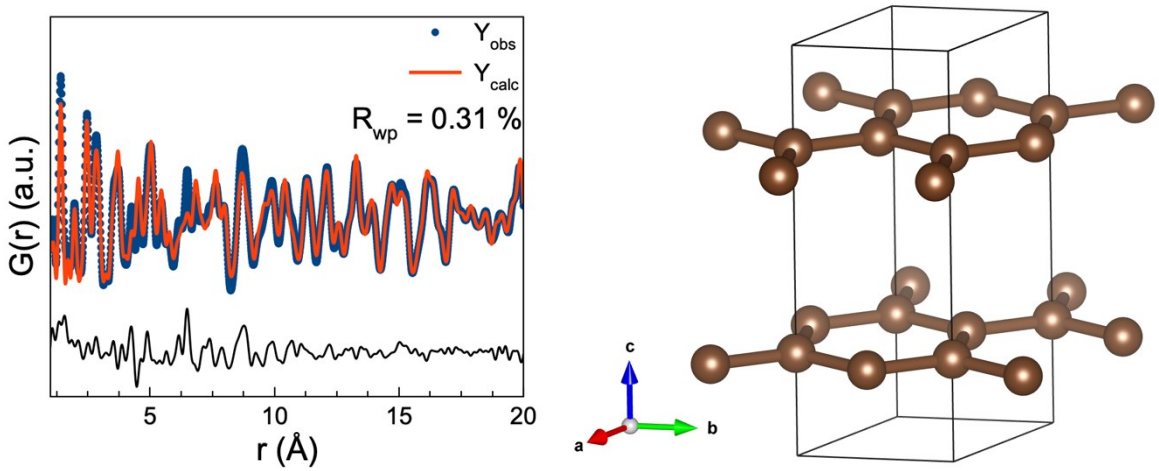

Figure S12: On the left is the fit of the local structure of the x = 0.2 sample using the 3 crystalline phases observed in the Rietveld refinement and a spherical graphite "nanoparticle" with a diameter of 7 Å. This graphite model can describe the local structure failed to be described by the crystalline phases. The graphite phase is not individual 7 Å nanoparticles, but instead the carbon species is more likely a disordered carbon phase which locally resembles graphite. On the right is the crystal structure of graphite.

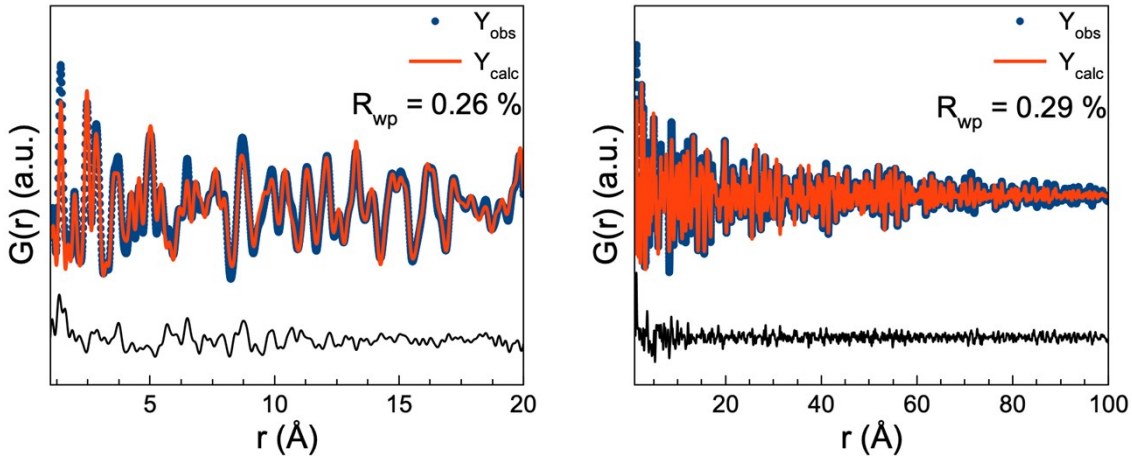

Figure S13: On the right is a fit where the carbon atoms have been allowed to move along the crystallographic c-axis in the graphite model to better describe the disordered carbon phase. On the left is the same fit but only fitted up to 20 Å. Letting the carbon atoms move along the crystallographic c-axis improves the fit and indicates that the graphite sheets are bend in the disordered carbon species.

Magnetic measurements

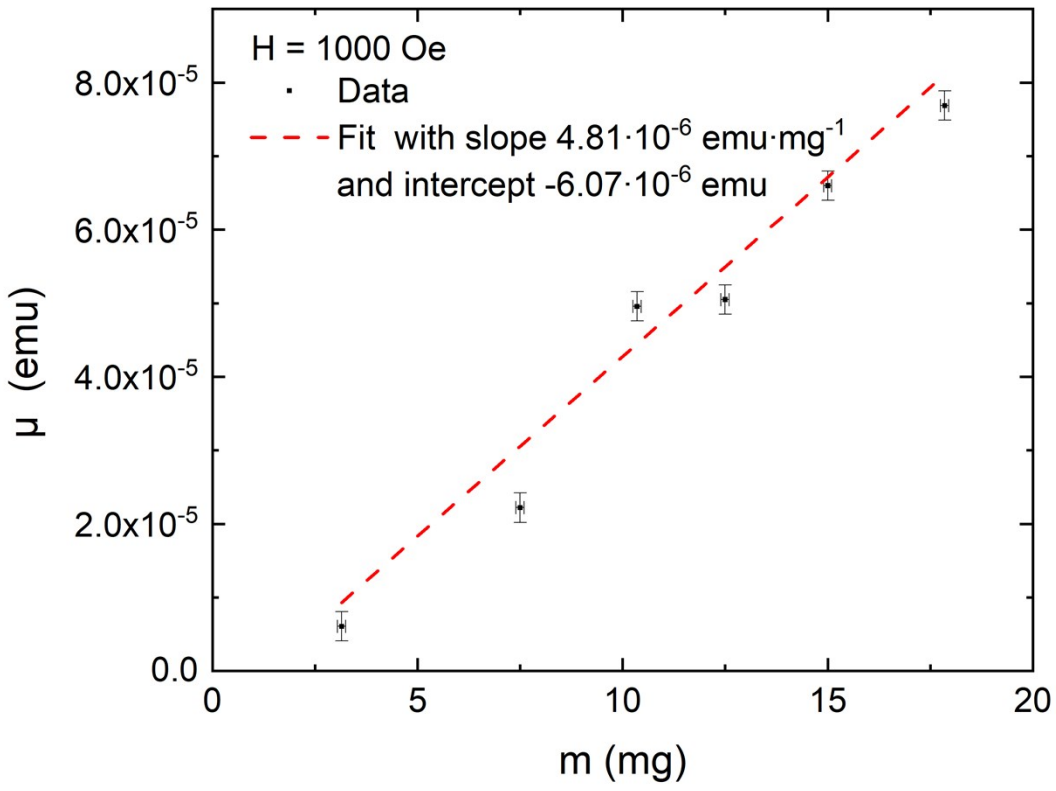

Figure S14: Total sample magnetic moment as function of $(Cr_{0.96}Mn_{0.04})_2GaC$ sample mass measured in the same capsule and linear fit of the six independent measurements. From the fit the sample magnetization can be extracted while the intercept is the capsule diamagnetic signal.

References

1. Coelho, A. A. TOPAS and TOPAS-Academic : an optimization program integrating computer algebra and crystallographic objects written in C++. *J. Appl. Crystallogr.* **51**, 210–218 (2018).
2. Jeitschko, W., Nowotny, H. & Benesovsky, F. Kohlenstoffhaltige ternäre Verbindungen (V-Ge-C, Nb-Ga-C, Ta-Ga-C, Ta-Ge-C, Cr-Ga-C und Cr-Ge-C). *Monatshefte für Chemie* **94**, 844–850 (1963).
3. Nanoscale-Ordered Materials Diffractometer, *PDF Data Analysis.* Retrieved from https://neutrons.ornl.gov/nomad/users Accessed August 2020
4. McDonnel, M. T. *et al.* ADDIE: ADvanced DIffraction Environment – A Software Environment for Analyzing Neutron Diffraction Data. *Acta Crystallogr. Sect. A* **73**, (2017).
5. P. Juhás and T. Davis, C. L. Farrow, S. J. L. Billinge, PDFgetX3: A rapid and highly automatable program for processing powder diffraction data into total scattering pair distribution functions, *J. Appl. Crystallogr.* **46**, 560-566
6. P. Juhás, J. N. Louwen, L. van Eijck, E. T. C. Vogt, S. J. L. Billinge, PDFgetN3: atomic pair distribution functions from neutron powder diffraction data using ad hoc corrections, *J. Appl. Crystallogr.*, **51**, 1492–1497 (2018